ACS Sustainable Chemistry & Engineering

Research Article

pubs.acs.org/journal/ascecg

# Nanoparticle Emission Characterization and Management in Nanocoating Material Spray Operation

Rohan G. Uttarwar and Yinlun Huang*

Department of Chemical Engineering and Materials Science, Wayne State University, Detroit, Michigan, 48202, United States

**ABSTRACT:** Nanoparticle emission occurs during nanomaterial manufacturing, application, and the use phase of the end product. Nanopaint is a very promising type of nanocoating material, in which nanoparticles are added into the resin of the paint. During paint spray, a certain fraction of paint unable to land on the surface of substrate will enter the environment. The nanoparticles contained in tiny paint droplets are thus emitted, which will fly in the air for a certain period of time, and then either land on the wall of the spray booth or follow the ventilation air flow to a drainage water system. To minimize the adverse environmental and health impact and to improve nanopaint transfer efficiency, the nanoparticle emission must be minimized and managed. In this paper, we introduce a CFD-based modeling and simulation approach to characterize nanoparticle transport dynamics and quantify nanoparticle emission. The models are incorporated into a comprehensive system model set that includes a process energy efficiency model and a product quality model that characterizes the formation of nanocoating film on substrates. The model set is then used to study the entire nanopaint spray operation, where coating quality, material and energy use efficiency, and emission minimization are characterized. Case studies will demonstrate the efficacy of the methodology with comparison of literature data.

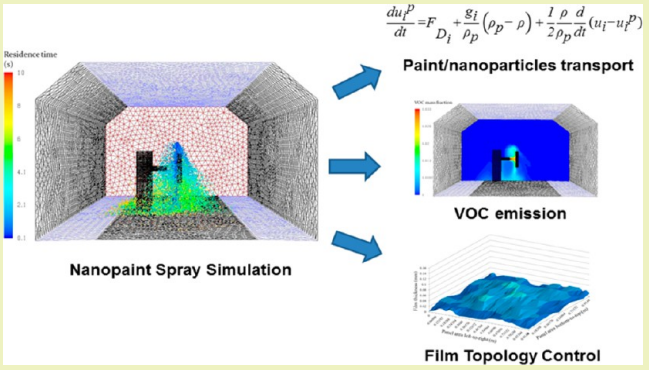


**KEYWORDS:** *Nanoparticle emission, VOC, Surface coating, Energy efficiency, CFD modeling*

## INTRODUCTION

Nanocomposite coating technology has become a rapidly expanding area of research. It encompasses a variety of systems with substantially improved properties and novel functionalities. Some of the existing nanocoatings show significantly enhanced barrier and mechanical properties, such as tensile strength, stiffness, elongation at break, impact strength, etc.[1,2] Some others exhibit improved flame retardancy and thermal resistance.[3] These materials become increasingly important because of their electrical and magnetic properties.[4] One of the obvious benefits of using nanocomposite coatings over conventional coatings is that all the superior properties can be achieved with typically 5−10% (by weight) loading of nanomaterials, while the conventional coatings may require 10−50% (by weight) loading of inorganic fillers into coating compositions. As a result of various advanced properties, nanoparticle coatings are finding numerous applications in automotive, aerospace, ship-making, security, chemical, electronics, steel, construction, and many other industries.[5]

With these numerous advantages, nanocoating technologies also come with certain drawbacks. The study of nanocomposite materials requires a multidisciplinary approach.[6] In spite of the research and investigation for years, no profound knowledge about their physico−chemical attributes that lead to the superior properties is available. Because of the existence of vast design parameters and experimental complexity, nanopaint design optimality is extremely difficult to address.

It is vital to look at the entire life cycle of nanopaint−nanocoating technology, which requires systematic analysis of the impact of the nanoparticles addition to conventional paint formulations. There have been serious concerns over the environmental and health issues associated with nanomaterials.[7] These environmental risks depend on the type and concentration of nanoparticles and exposed surrounding. Although there have been many studies on toxicology of nanoparticles,[8,9] the effect of nanopaint exposure and application has not been studied in detail. There exists a serious knowledge gap between the nanocomposite coatings potential and sustainability issues, which includes nanoparticle-related environmental threats as well as life cycle performance of nanocoating products and the overall performance in terms of energy use, safety, water use, waste emission, etc.

In automotive coating development, paint materials are applied via paint spray in order to generate a few layers of thin films on vehicle panels. This common application process requires a significant amount of energy and could cause serious

**Special Issue:** Sustainable Chemical Product and Process Engineering

**Received:** September 30, 2013
**Revised:** November 13, 2013
**Published:** November 21, 2013

  

environmental emission. The performance of paint spray has a direct effect on paint transfer efficiency, film topology, and nanoparticle/VOC emission, which have great impacts on the material and operating costs, product quality, environmental cleanness, and treatment cost.

A typical paint spray technique uses a compressed gas to atomize paint material and direct it at a high velocity to the receiving panel through spray guns.[10] Although most of the sprayed paint lands on the target, a certain amount of paint is carried by the ventilation air and enters the water in the drain through grids on the booth floor. In operation, the workers inside the spray booth may be exposed to severe conditions, such as exposure to VOCs, heat overload, electric shock or electrocution, noise, and other types of body injuries. It has been recognized that VOCs affect human health and productivity the most in the manual paint application process due to possible acute symptoms to workers, including headache, dizziness, and exposure to suspected carcinogens.[11,12]

For nanopaint, the overspray paint mist is laden with toxic nanoparticles and VOCs. It may severely pollute the booth air as well as the water flowing through the washout. Dunnett studied how the presence of contaminants and the air flow pattern affect workers' health.[13] If exposed to severe concentrations of toxic nanoparticles, such as nanosilica or nanotitanium dioxide, it can cause fatal health disorders.[14] Thus, it is important to develop an optimized paint spray operation, which would be more sustainable in terms of environmental emission, coating film quality, and high transfer efficiency.

Li et al. demonstrated the potential of CFD-based modeling methodology for the comprehensive analysis of a manual paint spray system.[15] It was shown that the spray booth geometry and operation parameters could be adjusted to control VOC emission below a threshold and to improve energy efficiency. However, the species transport model used in that study was unable to simulate the flow of liquid droplets through the spray booth. It was also not possible to simulate the flow of a multiphase fluid system, which is critical to studying nanopaint material spray. CFD modeling was also used to characterize the mass transfer and flow of VOC in the booth environment.[16,17] It was applied to simulate the breathing-zone concentration for a paint spray method in a simple spray booth unit with cross-flow ventilation.[16] Kim et al. analyzed a small-scale painting process with various exits of air leaving at different suction velocities.[12] Lu and Howarth presented numerical results of the prediction of air velocities, aerosol particle deposition, and migration in two interconnected ventilated zones.[18] Dunnett presented a study on the effect of the presence of workers on the air flow pattern and the factors affecting the exposure to contaminants. However, more systematic and quantitative VOC emission characterization and energy-efficient VOC reduction analysis for surface coating systems have not been thoroughly studied yet, and there has been no studies on nanoparticle emission in paint spray.

## PAINT SPRAY SYSTEM DESIGN

An automotive paint spray system consists of a spray booth, spray guns/bells, a ventilation system, tools, appliances, and equipment, such as a pump, compressor, conveyor belt, and personal protective gear, which are necessary for an operator to apply paint on the object surface to be coated. In operation, paint is sprayed by robotic manipulators. Paint particles are ejected toward the vehicle panels at a high speed. The efficiency of paint spray and the final coating film quality depends on several factors, such as the paint flow rate, paint injection velocity, atomization method, ventilation air velocity, spray angle, distance between gun and substrate, etc.[19] The overspray released during the painting operation is removed by the downdraft air that flows through the booth geometry and is absorbed by the water flowing underneath the exhaust grid. The removal of the overspray can be more efficient with a higher downdraft velocity of ventilation air, but this consumes more energy. To improve the process economy and coating film quality, high transfer efficiency is critical. While spraying nanopaint, the exposure to nanoparticles via different pathways, such as inhalation or dermal, can cause severe health hazards.[20] $TiO_2$, $SiO_2$, MMT clay, Al, etc. are among the most commonly used nanoparticles in coating formulations. Research has shown that exposure to high concentrations of such materials may result in possible acute symptoms to workers, including headache, dizziness, and exposure to suspected carcinogens, and sometimes this can also affect the central nervous system.[11,12]

For nanopaint, the paint particles are filled with individual or agglomerated nanoparticles inside it. The droplets containing nanoparticles are ejected from the bells at high speed to form a film on automotive panels. The transfer efficiency of water-borne paint material is generally around 30−40% while that of solvent-borne is 60−80%. The paint droplets not landing on the receiving panels are emitted into the surrounding atmosphere resulting in contamination of the air inside the spray booth. This contamination could include a noticeable concentration of nanoparticles and VOCs.

Figure 1 shows a typical manual spray booth design. The design consists of a paint spray booth with operational parameters adopted from a real industrial practice. The size of the booth that we studied is 19 ft by 39 ft, which is housed in a room of dimensions approximately 350 ft long and 60 ft wide. Inside the booth, a conveyor belt is located for moving parts through the working area. Paint is applied by a compressed air-forced paint gun operated by a worker positioned next to the substrate panel. After painting, the parts are carried out of the booth into dryers for flash-off and curing. The wet topcoat

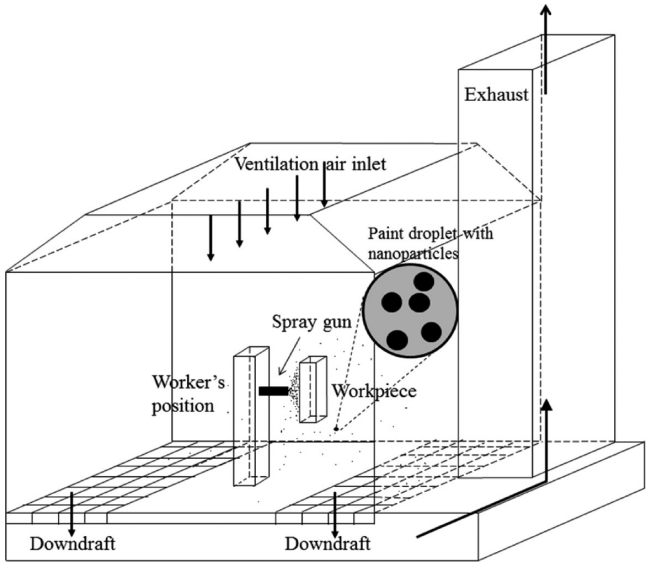


**Figure 1.** Sketch of manual paint spray booth.


dx.doi.org/10.1021/sc4003906 | ACS Sustainable Chem. Eng. 2014, 2, 95−105

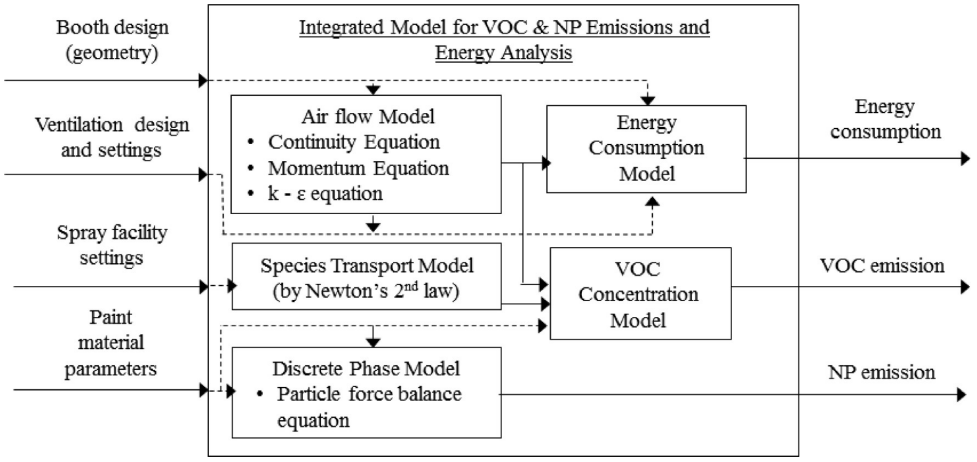


**Figure 2.** CFD-based integrated modeling methodology.

thickness is about 3 mils. A successful paint application job should produce a smooth, continuous, adherent, paint film free of runs, sags, blisters, orange peel, streaks, craters, blotches, fish eyes, and pinholes.

The roof of the paint booth is open and air is drawn through a 13 ft wide opening down to both exhaust air intakes with 4 ft wide slots located on each side of the booth floor. Four 25 horsepower motors power the exhaust fans to discharge paint fumes outdoor, which allows the exhaust air to flow at 80,000 CFM (cubic feet per minute). During the painting operation, fresh air enters the booth from the open roof and flows down to the floor continuously (Figure 1). Both ends of the booth are kept open. The heating and ventilation facility operates continuously at all times.

## INTEGRATED MODELING METHODOLOGY

The transport of ventilation air, shaping air, injected paint material, VOCs, and nanoparticles can be thoroughly examined through CFD-based modeling and simulation. Figure 2 represents a general scheme of the modeling methodology and different types of models that are used for the calculation of energy efficiency, VOC emission, and nanoparticle emission during the spray process. This methodology consists of five different models that are described below. Four of the models were used by Li et al. for the analysis of VOC emission and energy efficiency of a paint booth for conventional paint spray.[15] In this work, the discrete phase model is combined with the previous models to make it suitable for the analysis of nanoparticle-based paint systems.

**Air Flow Model.** The air flow pattern within the spray booth is determined by the geometry of the booth and ventilation system's design and setting. It can be characterized by the following dynamic models based on the mass conservation principle (eq 1) and the momentum conservation principle (eqs 2−4), as well as the realizable $k-\varepsilon$ turbulence principle (eqs 5 and 6).[10,21,22] The air is a continuous phase in the simulation. The prediction of flow of continuous phase is obtained through a realization $k-\varepsilon$ model. It is an improved turbulence model as compared to the previous standard $k-\varepsilon$ model.[23] The governing equations for these models are given below.

$$\frac{\partial}{\partial t}\rho_a = -\nabla \times (\rho_a v) + S_m \tag{1}$$

$$\frac{\partial}{\partial t}(\rho_a v) = -\nabla \times (\rho_a vv) - \nabla p + \nabla \times \tau + \rho_a g + \sum_i \langle \dot{S}_i \rangle \tag{2}$$

where

$$\tau = (\mu_a + \mu_t)(\nabla v + \nabla(v)^T) - \frac{2}{3}(\mu_a + \mu_t)(\nabla \times v)I \tag{3}$$

$$\mu_t = \rho_a C_\mu \frac{(k)^2}{\varepsilon} \tag{4}$$

and

$$\frac{\partial}{\partial t}(\rho_a k) = -\nabla \times (\rho_a vk) + \nabla \times \left[\left(\mu_a + \frac{\mu_t}{\sigma_k}\right)\nabla k\right] + G_k + G_b - \rho_a \varepsilon - Y_M \tag{5}$$

$$\frac{\partial}{\partial t}(\rho_a \varepsilon) = -\nabla \times (\rho_a v\varepsilon) + \nabla \times \left[\left(\mu_a + \frac{\mu_t}{\sigma_\varepsilon}\right)\nabla \varepsilon\right] + C_{1\varepsilon}\frac{\varepsilon}{k}C_{3\varepsilon}G_b + C_1\rho_a S_\varepsilon - C_2\rho_a \frac{\varepsilon^2}{k + \sqrt{v\varepsilon}} \tag{6}$$

where $\rho_a$ is the air density (kg/m$^3$); $v$ is the velocity of air (m/s); $S_m$ is the rate of mass addition into the gas phase per unit volume from the dispersed second phase (kg/m$^3$s); $p$ is the pressure (Pa); $\tau$ is the stress tensor of the air (Pa); $g$ is the acceleration due to gravity (m/s$^2$); $\dot{S}_i$ is the external force on gas phase per unit volume from the $i$-th species particle (N/m$^3$); $\mu_a$ and $\mu_t$ are, respectively, the shear viscosity (Ns/m$^2$) and turbulent viscosity (Ns/m$^2$); $I$ is the unit tensor, $C_\mu$, $C_{1\varepsilon}$, $C_{2\varepsilon}$, $C_{3\varepsilon}$, and $\sigma_k$ are the model constants; $k$ is the kinetic energy of turbulence (m$^2$/s$^2$); $\varepsilon$ is the dissipation rate of turbulence (m$^2$/s$^3$); $G_k$ is the generation of turbulent kinetic energy due to the mean velocity gradient (kg/ms$^3$); $G_b$ is the generation of turbulent kinetic energy due to buoyancy (kg/ms$^3$), and $Y_M$ is the contribution of the fluctuating dilatation in compressible turbulence to the overall dissipation rate (kg/ms$^3$). More details about the realizable $k-\varepsilon$ model can be found in the ANSYS FLUENT theory guide.[24]

The air within the spray booth is initially static. The fresh air then begins to blow from the booth intake to the exhaust. It is interfered by the shaping air flow near the spray guns. The air flows out of the booth to the environment through exhaust


dx.doi.org/10.1021/sc4003906 | ACS Sustainable Chem. Eng. 2014, 2, 95−105

grids located on the floor. These operating conditions inside the spray booth are defined by the following initial and boundary settings of the air flow model.

$$v(x,t) = \begin{cases} v_{SG} \text{ at the outlet of spray guns, } t > 0 \\ v_{DD} \text{ at booth intakes, } t > 0 \\ 0 \text{ at other physical boundaries except the exhausts, } t > 0 \\ 0 \text{ in the spray booth, } t = 0 \end{cases} \quad (7)$$

where $v_{SG}$ is the air velocity from the spray gun (m/s), and $v_{DD}$ is the air velocity of the downdraft (m/s).

**Species Transport Model.** Paint particles are ejected from the spray guns with a momentum that is governed by two types of forces: the drag force from the surrounding turbulent air flow and the gravitational force. The velocity of paint species ($u$) can be modeled by the Newton's second law of motion as shown in the following equations.[10,25]

$$\frac{du(t)}{dt} = \frac{3\pi\mu_a D_p}{m}(v(t) - u(t))f + g \quad (8)$$

where

$$m = \frac{1}{6}\pi(D_p)^3\rho_p \quad (9)$$

$$f = \begin{cases} 1 + \frac{(Re_r)^{2/3}}{6}, & Re_r < 1000 \\ 0.0183Re_r, & 1000 \le Re_r \le 3 \times 10^5 \end{cases} \quad (10)$$

$$Re_r = \frac{D_p|v(t) - u(t)|\rho_a}{\mu_a} \quad (11)$$

where $u$ (m/s) is the velocity of the species having particle diameter $D_p$ (m) and mass $m$ (kg), $v$ (m/s) is the velocity of air surrounding the species, $f$ is the drag factor, $\rho_p$ is the paint density (kg/m$^3$), and $Re_r$ is the Reynolds number.

The initial species velocity from the spray guns for this model is $u_0$, i.e.,

$$u(0) = u_0 \quad (12)$$

The species trajectory $x_{tr}(t)$ is determined from the species velocity that is determined by eqs 8−12. The initial position of all paint species is assumed to be at the outlet of the spray gun. The dynamic model becomes

$$\frac{dx_{tr}(t)}{dt} = u(t) \quad (13)$$

$$x_{tr}(0) = x_0 \quad (14)$$

The models for the air flow and the species transport can be solved numerically. The solution can be obtained at various locations within the booth and at different times. The results from the CFD simulation can characterize the emission and diffusion of VOCs in the system as well as the effect of ventilation during the paint spray operation.

## VOC CONCENTRATION MODEL

The air quality inside the spray booth is quantified by measuring the mean VOC concentration ($C_m$, kg/m$^3$) in the system; which is the ratio of total mass of VOCs to the total space of the booth ($V_{bh}$, m$^3$).

$$C_m = \frac{\int_{V_{bh}} Y\rho_s dV}{V_{bh}} \quad (15)$$

where $\rho_s$ is the species flow density (kg/m$^3$) obtained from the species transport model, and $Y$ is the mass fraction of VOC in the paint species flow. This model accounts for the VOC content released in the air from the paint being applied onto the substrate and also the overspray. The VOC evaporation from the deposited wet film is neglected as the substrate is immediately moved from the paint booth to the next production stage.

**Energy Consumption Model.** In paint spray operation, energy is consumed by exhaust fans that provide ventilation air and by the spray facilities that generate the shaping air. Industrial practice shows that maintaining ventilation air flows consumes much more power than keeping shaping air flows. Thus, in this work, the total energy consumption of a paint spray system is quantified solely using the energy consumed by the ventilation system. The power required for the exhaust fans ($E_d$, kW) is proportional to the velocity of the exhaust air flow ($v_{DD}$, m/s),[26] i.e.,

$$E_d = cv_{DD} \quad (16)$$

where $c$ is a given coefficient (kW/m/s).

**Discrete Phase Model.** In addition to solving the transport equations of the continuous phase, FLUENT also provides a tool for simulating the discrete second phase. The paint acts as a discrete second phase, which is sprayed in a continuous air domain. The dispersed phase can exchange mass, momentum, and energy with the continuous phase. It is treated by the Lagrangian discrete phase model (DPM), which follows the Euler−Lagrange approach. The DPM is combined with the species transport model to calculate the paint flow trajectories and nanoparticle emission (Figure 2). This discrete phase is sprayed in the form of a large number of tiny particles representing real paint droplets with the same properties. By this representation, one can control the size distribution of paint droplets that are being injected from the gun. The droplets are traced through the booth environment at each time interval of iteration. The trajectory of the individual droplet is determined by solving the equation of motion for each droplet. This equation of motion is obtained from the particle force balance written in a Lagrangian frame of reference (eq 17). This equation considers the forces in the $i^{th}$ direction of Cartesian coordinates due to drag, gravity, and pressure gradient. The thermophoretic and Brownian motion forces are neglected.

$$\frac{du_i^p}{dt} = F_{D_i} + \frac{g_i}{\rho_p}(\rho_p - \rho) + \frac{1}{2}\frac{\rho}{\rho_p}\frac{d}{dt}(u_i - u_i^p) \quad (17)$$

where

$$F_{D_i} = \frac{18\mu}{\rho_p d_p^2}\frac{C_D R_e|u_i^p - u_i|}{24} \quad (18)$$

$$R_e = \frac{\rho d_p|u_i^p - u_i|}{\mu} \quad (19)$$

where $F_{D_i}$ is the drag force per unit particle mass; $u_i$ and $u_i^p$ are the velocities of fluid phase and particles, respectively; $\rho$ and $\rho_p$ are the densities of the fluid phase and particles; respectively;


dx.doi.org/10.1021/sc4003906 | ACS Sustainable Chem. Eng. 2014, 2, 95−105

**Table 1. Material Properties of Various Paint Systems**

| parameters | nanopaint I | nanopaint II | conventional paint |
|---|---|---|---|
| paint density (g/cm$^3$) | 1.286 | 1.286 | 1.23 |
| NP type | $SiO_2$ with 100 nm particle size | | N/A |
| NP mass fraction (%) | 10 | 5 | 0 |
| viscosity (cP) | 46 | 43 | 40 |
| paint flow rate (mL/min) | 150 | 150 | 150 |
| size of paint droplets ($\mu$m) | 10−100 | 10−100 | 10−100 |
| solvent (acetone) concentration (lb/gal) | 4 | 4 | 4 |

$C_D$ is the drag coefficient; $d_p$ is the particle/droplet diameter; $\mu$ is the viscosity of the discrete phase; $g_i$ is the acceleration due to gravity; and $R_e$ is the Reynolds number.

During nanopaint spray, the nanoparticles are not released in the natural form but are surrounded with resin material. Essentially, the overspray paint mist carries the nanoparticles in the booth environment. The emission of nanoparticles thus depends upon the paint droplet size and the concentration of the overspray. The simulation of a mixture of species is accomplished by activating the FLUENT multicomponent particle law. It allows FLUENT to model each droplet consisting of multiple components with different masses and densities. The injected particles are allowed to collide or break on interaction with each other in the air and on the deposited film. The mass of each paint droplet changes depending upon the evaporation of solvent and collision and break-up phenomena. Droplet spreading on the substrate film depends on multiple factors, such as droplet size, injection speed, angle of impact, paint surface tension, viscosity, and surface properties (i.e., surface energy, surface roughness, porosity). The amount of deposition and spreading is determined by the driving force and the resistive force. The driving force is provided by the kinetic energy of the droplet, whereas the resistive force is provided by the viscosity and surface tension of the paint material. When the droplet impacts the surface, its initial spherical shape may change into an oval-like form. In FLUENT, the variation in the droplet shape is accounted by the "dynamic drag model". The distortion of shape significantly affects the drag coefficient of the droplet, and the value changes significantly from the drag coefficient of the spherical droplet. The dynamic drag model calculates the drag coefficient depending on the extent of distortion as given by eq 20.

$$C_D = C_{D,\text{sphere}}(1 + 2.632y) \tag{20}$$

where $y$ is the extent of droplet distortion from spherical to the maximum of disc-like shape. In the case of zero distortion ($y$ = 0), the drag coefficient of a sphere is used, while the maximum distortion ($y$ = 1) produces the drag coefficient of a disc shape.

## PAINT MATERIAL SPECIFICATION

The paint booth geometry for the base case was adopted from an industrial example.[15] Because nanopaint could be first used for developing a clearcoat, in this work, the paint material selected for modeling was an epoxy-based clearcoat resin, product no. D.E.R. 538.[27] For the nanopaint formulation, silicon dioxide nanoparticles of uniform size distribution of 100 nm were dispersed into the coating matrix.[28] The solvent used for all paint formulations was acetone. On the basis of the industrial data, the paint flow rate was selected as 150 mL/min.[25] The shaping air flow rate from the spray gun is set to 5 m/s. Such a high value of shaping air flow avoids the coating spray quality from getting affected by the downdraft ventilation air. The paint droplets were injected at a high velocity of 20 m/s. For the simulation and analysis of the paint spray through DPM, three paint systems were selected: (1) nanopaint I (with 10 wt % of nanoparticles), (2) nanopaint II (with 5 wt % of nanoparticles), and (3) conventional paint. The solvent concentration and material parameters of all three systems are listed in Table 1.

For the ventilation air unit, the booth was provided with four 25 hp fan motors. The flow rate of the exhaust air generated by the fans was 80,000 CFM. Thus, the exhaust air velocity was calculated as

$$\begin{aligned} v &= 80,000 \text{ CFM}/312 \text{ ft}^2 \\ &= 256.4 \text{ FPM (feet per minute)} \\ &= 1.30 \text{m/s} \end{aligned} \tag{21}$$

Note that the total intake area for the exhaust air is 312 ft$^3$ (i.e., 2 ft × 4 ft × 39 ft). The specified system information was used to construct the CFD-based models by employing eqs 1−16. The spray booth consists of four 25 hp fan motors, and the electrical draw of each motor is 18.64 kW. Thus, the energy coefficient in eq 16 is calculated as

$$c = 4 \times 18.64 \text{ kW}/1.30 \text{ m/s} = 57.35 \text{ kW/m/s} \tag{22}$$

The performance of the paint spray system, in terms of air purification by ventilation, quality of the deposited paint film, and transfer efficiency, depends on multiple factors, such as ventilation air velocity, shaping air velocity, spray pattern, injection tracks, injection angle, surface roughness, gun-to-substrate distance of separation, etc. For nanopaint spray, toxic nanoparticles are released in the atmosphere, which must be removed to keep the booth environment safe for workers. The quality of the film may alter due to the addition of nanoparticles in the paint matrix. The prediction of the coating film topology provides key information about the role of nanoparticles. For the process to be economical, the transfer efficiency of the paint is a crucial factor. All the parameters are a function of the method of spraying and operational settings. The optimum performance can be obtained by adjusting the operational parameters appropriately for each type of coating material to be used. This work studies these crucial operational parameters, which can improve the sustainability performance of the paint spray system for different types of coating materials.

## CASE STUDY

In this work, the paint material was applied on the panel surface with three different spray patterns. The spray patterns are described below as Cases 1 to 3. In each case, the separation between the gun and the substrate was fixed at 8 in. The performance of each of the three paint systems was analyzed through CFD-based modeling and simulation to compare the film quality, topological properties, and emission of NPs and

VOCs. The spray patterns and resulting coverage of the sample by the paint material are shown in Figure 3.

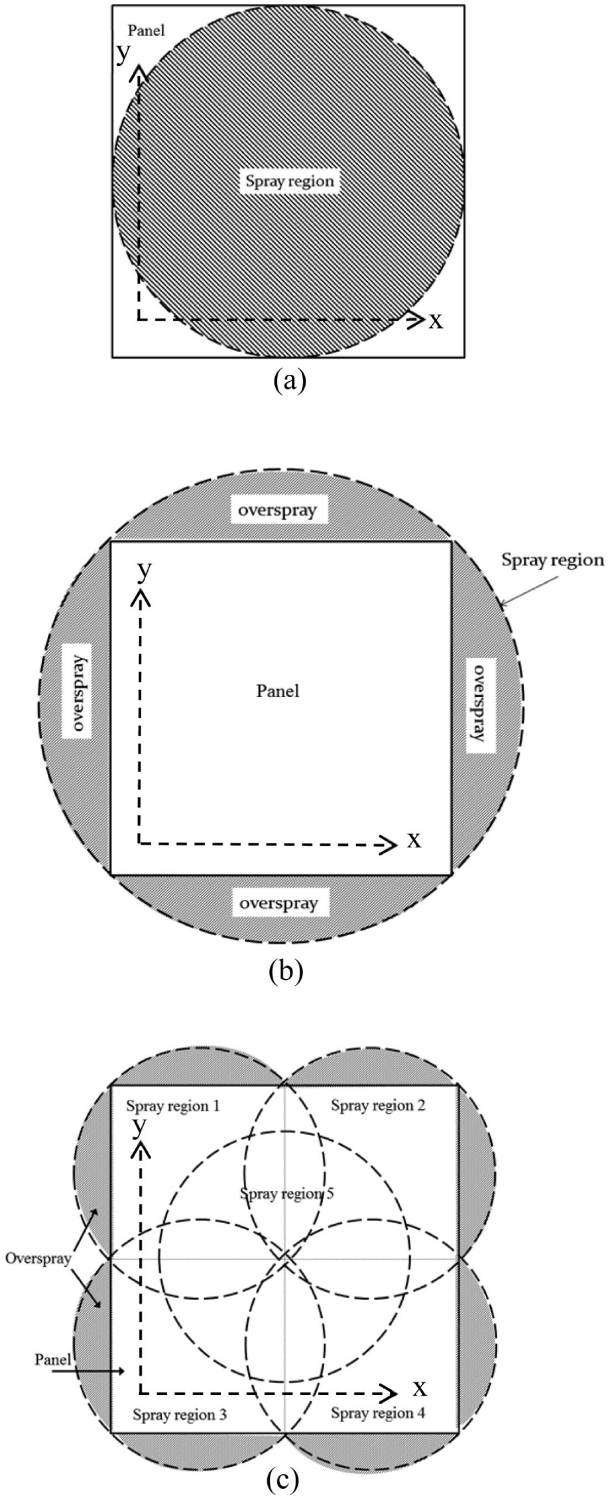


**Figure 3.** Spray patterns for (a) Case 1, (b) Case 2, and (c) Case 3.

Case 1: The paint was sprayed in a cone shape at the center of the sample at a spray angle of 66.02°. The spray angle was adjusted such that no paint could be released directly in the surrounding (Figure 3(a)).

Case 2: The paint was sprayed in a cone shape from the center at a spray angle of 71.67°. This spray angle ensured a complete coverage of the panel surface. However, a certain portion of paint was allowed to release directly in the surrounding as overspray (Figure 3(b)).

Case 3: The paint was sprayed at five different locations on the panel for 2 s at each at a fixed spray angle of 58°. The location of spray gun was changed to four corners and the center of the panel (Figure 3(c)) in order to improve the surface topology of the deposited film.

In each case, the paint was sprayed for 10 s. The paint was injected along 500 droplet streams from the outlet of the gun. The streams injected droplets of different diameters ranging from 10 to 100 $\mu$m. The intermediate droplet size distribution was calculated by applying Rosin−Rammler distribution function with 50 $\mu$m as the average size.[29] The spread parameter was set equal to 2. The Rosin−Rammler distribution function calculates the droplet sizes based on eq 23.

$$Y_d = e^{-(d/\bar{d})^n} \tag{23}$$

where $Y_d$ is the mass fraction of the paint material injected in the form of droplets with diameter $d$, $\bar{d}$ is the average diameter, and $n$ is the spread parameter. The plot of initial size distribution based on Rosin−Rammler equation is given in Figure 4.

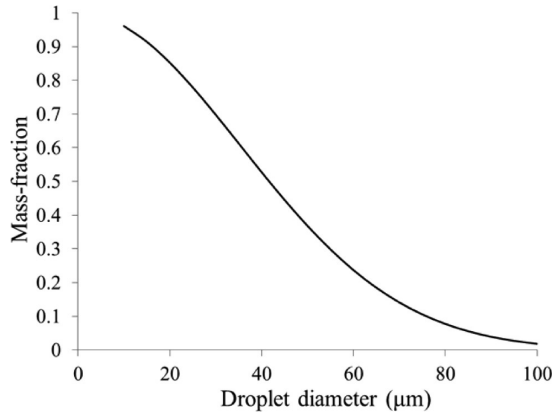


**Figure 4.** Initial droplet size distribution based on Rosin−Rammler function.

The CFD model of the paint spray system considered certain assumptions for the analysis of each case. These assumptions are as follows: (1) The nanoparticles were emitted in the atmosphere in the enclosed form inside a paint resin. (2) All the nanoparticles were spherical with identical size of 100 nm. (3) On collision of paint droplets on the substrate, the droplets showed one of the four behaviors: splash, spread, stick, and rebound. In the case of splashing, each droplet would break to form four tiny fractions of same size and equal mass fractions. (3) The effect of gravitational force, which may cause sagging of wet film was neglected. (4) The collision on walls of the paint booth leads to sticking of the paint material.

**Simulation Details.** The models described above were implemented using the ANSYS CFD software FLUENT, version 14. A fine mesh was generated with 356,746 total elements. The mesh resolution near the gun outlet was higher to accurately predict the flow dynamics and the interaction between spray particles and the air. The droplets were injected in a conical fashion from the spray gun. Unsteady particle tracking was applied for DPM particle treatment. The particles were sprayed at each particle time step of 0.1 s. Droplet


dx.doi.org/10.1021/sc4003906 | ACS Sustainable Chem. Eng. 2014, 2, 95−105

collision and droplet break-up (WAVE) models were activated to simulate the paint flow behavior during the spray. Stochastic tracking was applied by discrete random walk model. Coupled scheme was implemented for pressure−velocity coupling. The pressure discretization was performed under the second-order scheme.

The air flow model predicted the air flow profile inside the booth, which was generated as a result of interaction of downdraft air and shaping air. The contour of air flow velocity is shown in Figure 5.

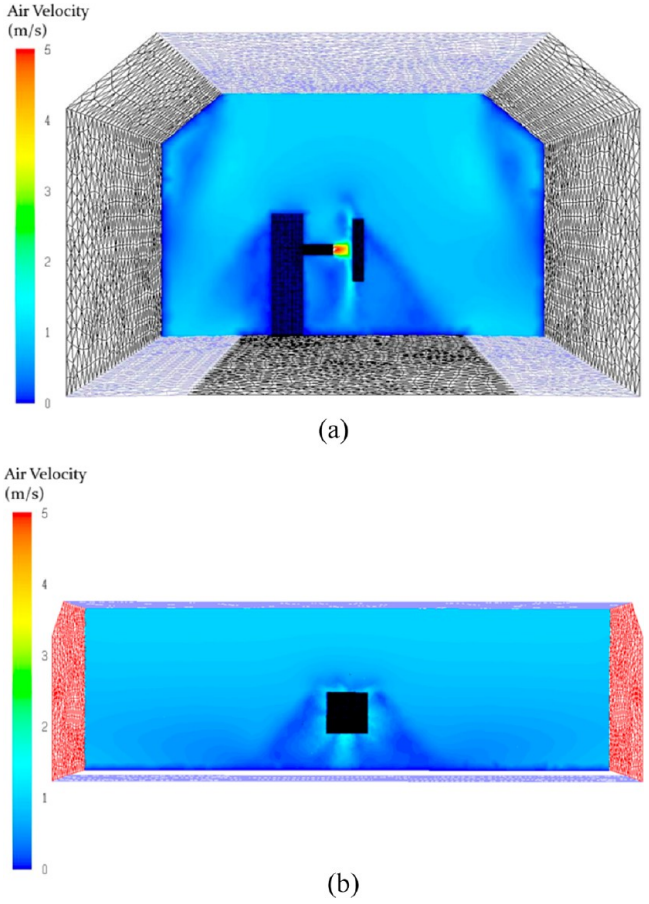


**Figure 5.** Air velocity contour (a) front view and (b) side view.

## RESULTS AND DISCUSSION

The paint spray booth was modeled, and the flow of paint throughout the booth area was analyzed by using CFD simulations. The paint spray of various samples through the developed case studies was analyzed for the assessment of environmental emission of VOCs and NPs as well as the surface topology change.

**Spray Trajectories Analysis.** The paint droplets were injected from the gun nozzle at a high speed of 20 m/s. Because of such high speed, the continuous phase had minimal effects on the flow and transfer efficiency of the paint. For the DPM simulation, the boundary condition for the walls of the booth was selected such that the droplets would stick after the contact. The downdraft air was allowed to flow from the opening on the roof to the grids mounted at the floor of the booth. The panel surface was set as "wall-film". The trajectories were calculated at every 0.1 s of iteration time step. In all the cases, the droplets ejected from the gun were either deposited on the panel or released in the air.

The flow of paint droplets along the spray booth is represented in Figure 6. It is shown in Figure 6(a) that the

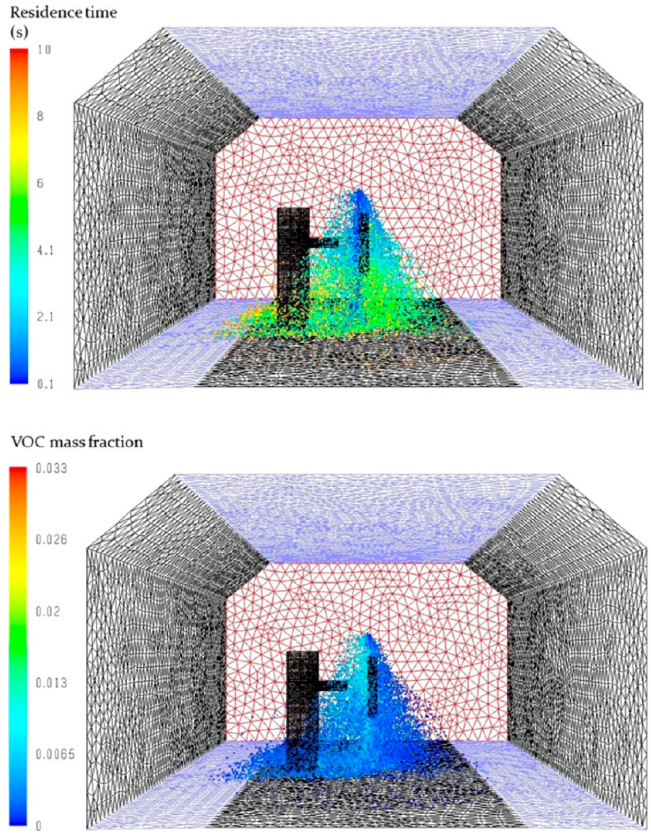


**Figure 6.** DPM droplet tracks at the end of 10 s of paint spray as a function of (a) residence time, and (b) VOC mass fraction.

particles with highest residence time (red color) are lying on the wall of the booth. However, the particles with smallest residence time (blue color) are observed near the panel. Figure 6(b) represents the paint particles in the air at the end of 10 s of spray and as a function of VOC content present in them. The coloring shows that the particles that are further away from the substrate and have spent a longer time in the booth have a lesser amount of VOCs in them. This is expected due to higher evaporation of solvents at the longer residence time.

**VOC Emission Analysis.** During the spray application, the solvent was continuously evaporating from the paint material. This VOC vapor contributes to the increasing air pollution inside the booth that could be hazardous to the worker standing inside. Using this CFD simulation for all the cases, the vaporized VOC concentration distribution was analyzed. Figure 7 represents this concentration of VOC. It can be seen that the vapor concentration is highest near the sample. This VOC vapor is taken away with the downdraft air through the grids at the bottom. The spray booth and ventilation system efficiency is determined by its ability to remove this VOC from the booth ambience and keep the environment clean for working.

The VOC emission was also analyzed more precisely by calculating the solvent concentration remaining inside 20 randomly selected droplet streams injected initially at a time zero. Figure 8 represents the trend of solvent concentration change in each of the 20 droplet streams of Case 1 for all three


dx.doi.org/10.1021/sc4003906 | ACS Sustainable Chem. Eng. 2014, 2, 95−105

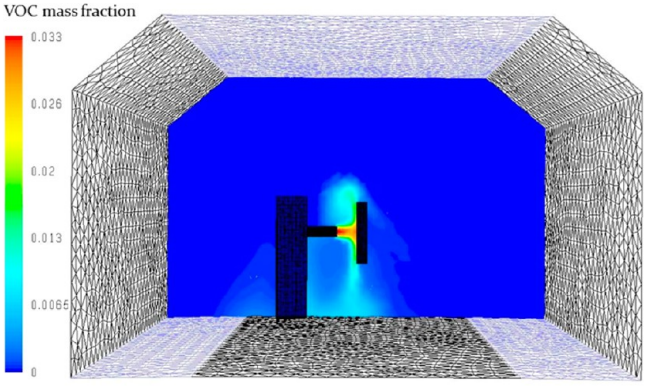


**Figure 7.** Concentration of VOC vapor inside the spray booth after 10 s of spray.

paint samples. It can be observed that the solvent concentration was exponentially decreasing along with the time. This decrease was a result of continuous solvent evaporation contributing to the increase in VOCs in the booth. The occasional increase in the solvent concentration of few droplets could be caused due to coalescence of several droplets together after depositing on the panel film (for example, particle 8). The majority of the droplet streams did not reach 10 s. This could also be a cause of coalescence of the droplets with others and spreading on the panel film. A close similarity among all three graphs (Figures 8(a–c) suggests that addition of nanoparticles in the paint matrix did not affect the solvent concentration trends of all the droplet streams. Thus, nanoparticles had negligible effect on VOC evaporation during the paint spray.

The deposition of the solvent on the panel surface was also analyzed and compared to study the effect of the nanoparticles addition into the coating matrix. Figure 9 represents the contours of solvent concentration that was deposited on the panel surface after the spraying of nanopaint I and conventional paint material through the spray pattern used in Case 1. The close proximity of the two contours suggests that nanoparticles have a negligible effect on the solvent deposition on the spray panel surface.

**Paint Transfer Efficiency.** The paint spray process can be economical, and the quality of the deposited paint film can be improved with an increasing transfer efficiency. Although spray painting provides good control over the quality of the finish, lower transfer efficiency may cause higher emission of paint mists. The transfer efficiency of the spray process primarily depends upon the injection speed and the gun-to-substrate separation distance. The nontransferred paint contributes to the overspray that causes workers' exposure to higher concentrations of paint mist.

The separation distance between the gun and sample was fixed to 8 in. for all the cases. The transfer efficiencies of all the cases and types of paints are reported in the Table 2. As expected, Case 1 provided the highest transfer efficiency followed by Case 3 and Case 2. It can be observed that the nanopaint samples with increasing nanoparticle concentration have better transfer efficiencies. This could be due to the presence of nanoparticles and an increase in paint viscosity. The spray of more viscous paint deposited more content on the film and formed lesser paint mist.

The overspray, consisting of paint solids, nanoparticles, and VOCs, results in the workers' exposure to toxic substances. This overspray must be removed efficiently by the downdraft

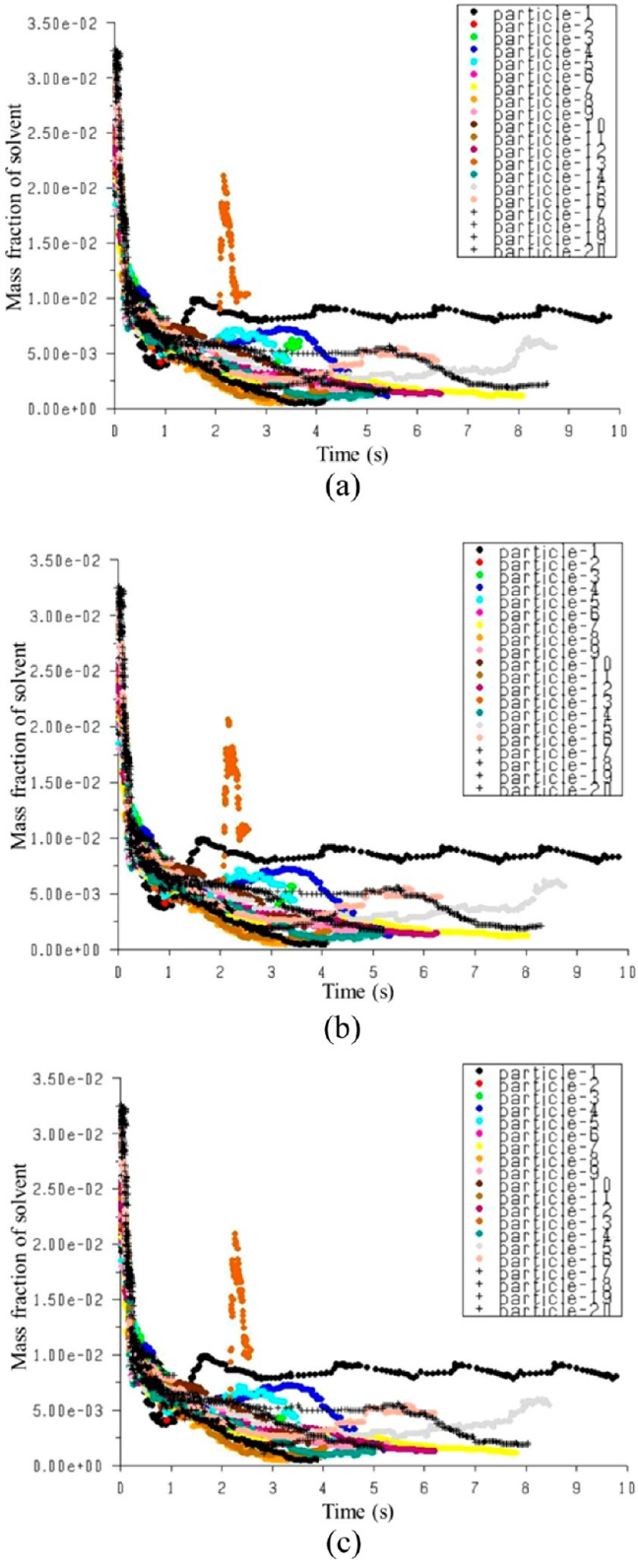


**Figure 8.** Solvent concentration change during the spray operation of Case 1 for (a) nanopaint I, (b) nanopaint II, and (c) conventional paint.

air in order to keep the booth environment safe for working. For all the simulated cases, the mass flow and velocity of downdraft air was kept unchanged. The efficiency of the ventilation system for different cases of paint systems was


dx.doi.org/10.1021/sc4003906 | ACS Sustainable Chem. Eng. 2014, 2, 95–105

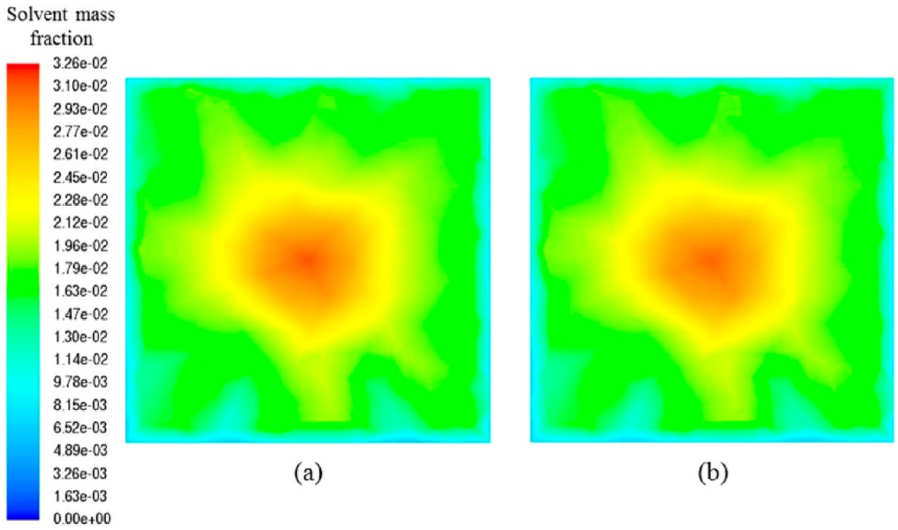


**Figure 9.** Contours of solvent deposition on the panel surface by the spray pattern of Case 1 for the spraying of (a) nanopaint I and (b) conventional paint.

**Table 2. Analysis of Performance Parameters for All Three Cases of Paint Spray**

| parameter | cases | geometry and spray pattern | nanopaint I | nanopaint II | conventional paint |
|---|---|---|---|---|---|
| transfer efficiency (%) | 1 | spray at the center (partial coverage of panel) | 85.09 | 81.73 | 74.93 |
| | 2 | spray at the center (full coverage of panel) | 74.85 | 73.86 | 72.05 |
| | 3 | spray at five locations (full coverage of panel) | 80.91 | 76.46 | 72.26 |
| paint removed by the ventilation system (%) | 1 | spray at the center (partial coverage of panel) | 31.48 | 31.09 | 32.02 |
| | 2 | spray at the center (full coverage of panel) | 30.61 | 30.71 | 31.07 |
| | 3 | spray at five locations (full coverage of panel) | 31.12 | 31.08 | 32.45 |
| NPs concentration in booth air (no./m$^3$) | 1 | spray at the center (partial coverage of panel) | $1.351 \times 10^{12}$ | $8.323 \times 10^{11}$ | 0 |
| | 2 | spray at the center (full coverage of panel) | $2.307 \times 10^{12}$ | $1.197 \times 10^{12}$ | 0 |
| | 3 | spray at five locations (full coverage of panel) | $1.742 \times 10^{12}$ | $1.074 \times 10^{12}$ | 0 |

**Table 3. Average Film Thickness and Roughness Values for All Cases of All Paint Samples**

| | average film thickness ($\mu$m) | | | arithmetic mean roughness ($\mu$m) | | |
|---|---|---|---|---|---|---|
| cases | nanopaint I | nanopaint II | conventional paint | nanopaint I | nanopaint II | conventional paint |
| 1 | 29.70 | 28.54 | 25.43 | 22.26 | 21.93 | 18.86 |
| 2 | 25.55 | 24.55 | 24.28 | 14.25 | 14.11 | 15.34 |
| 3 | 27.31 | 26.17 | 24.30 | 8.47 | 8.16 | 7.79 |

**Table 4. Theoretical Thickness Values and Percent Error in Calculations for All Simulation Cases**

| parameter | cases | geometry and spray pattern | nanopaint I | nanopaint II | conventional paint |
|---|---|---|---|---|---|
| transfer efficiency (%) | 1 | spray at the center (partial coverage of panel) | 85.09 | 81.73 | 74.93 |
| | 2 | spray at the center (full coverage of panel) | 74.85 | 73.86 | 72.05 |
| | 3 | spray at five locations (full coverage of panel) | 80.91 | 76.46 | 72.26 |
| theoretical thickness ($\mu$m) | 1 | spray at the center (partial coverage of panel) | 29.68 | 28.50 | 27.32 |
| | 2 | spray at the center (full coverage of panel) | 26.11 | 25.76 | 26.27 |
| | 3 | spray at five locations (full coverage of panel) | 28.22 | 26.67 | 26.35 |
| % error | 1 | spray at the center (partial coverage of panel) | 0.08 | 0.14 | 3.24 |
| | 2 | spray at the center (full coverage of panel) | 2.11 | 4.71 | 7.58 |
| | 3 | spray at five locations (full coverage of panel) | 4.64 | 3.36 | 7.78 |

studied by calculating the proportion of paint removed by the downdraft air out of total overspray. The corresponding values are reported in Table 2. It confers that the efficiency of the ventilation system, in the case of conventional paint, is slightly better than that of nanopaint. However, it is preferred to have a high efficiency of ventilation system, especially in the presence of toxic nanoparticles. Thus, there is a trade-off between the transfer efficiency and environmental emission.

**Nanoparticle Emission.** The nanoparticle emission during each case was analyzed by calculating the total concentration of nanoparticles in the booth environment at the end of paint spray operation. The values obtained from the analysis are reported in Table 2. It is shown that the higher nanoparticles content in the paint system invites further risk of nanoparticle emission and exposure to higher concentrations. Highest concentration of nanoparticles was emitted during the spray


dx.doi.org/10.1021/sc4003906 | ACS Sustainable Chem. Eng. 2014, 2, 95−105

of nanopaint samples through Case 2. With the environmental regulations on nanoparticle emission becoming more strict day-by-day, it is crucial to have an optimized ventilation system for nanopaint spray to minimize this exposure that can cause several health concerns.

**Film Topology Analysis.** The key benefit of the paint spray application method is the ability to control and improve surface morphology and coating film topology. Spreading of the paint material on the film and the prediction of velocity profiles of paint droplets are the fundamental factors required for the accurate determination of surface morphology. Fogliati et al. determined that the Realizable $k-\varepsilon$ model gives most accurate prediction of these characteristics.[17] Thus, the same model was adopted for the simulation of all the cases.

In order to determine the film thickness profile of the deposited paint layer, the sample surface was modeled as a "wall-film", which predicts four different phenomena of spread, stick, rebound, and splash of the impacting paint droplets depending on the impact angle and velocity. The paint mass and deposited film thickness values at various locations on the panel were recorded. Using these values, the plots of distribution of paint thicknesses over the panel surface were reconstructed and analyzed. The plots obtained for the spray of nanopaint I using all three cases of spray patterns are represented in Figure 10.

The roughness of the film surface was calculated as the "arithmetic mean roughness ($R_{mean}$)" by using eq 24.

$$R_{mean} = \frac{1}{n}\sum_{i=0}^{n} |y_i| \tag{24}$$

where $y_i$ is the vertical distance from the mean thickness line to the $i^{th}$ data point, and $n$ is the number of selected ordered and equally spaced data points along the surface of the panel. The values of the average thickness and roughness of the deposited film from all the cases are reported in Table 3. In order to ensure the reliability of the simulations and the accuracy of the thickness data, these average thickness values were compared with the theoretically calculated thickness values. The theoretical thickness is the ratio of quantity of paint that is transferred on the substrate over the cross sectional area of the substrate. The final values were calculated for each case, and the percent error is reported in Table 4. For all the cases, the error was less than 8%, which verified the reliability of the simulation and the final results.

From Figure 10, it can be observed that the film topology from Case 3 was substantially improved as compared to that from Case 1 and Case 2. The thickness values from Table 3 suggest that the average thicknesses of nanopaint samples were greater than the conventional paint. Case 3 showed about a 7% improvement in the average film thickness than the worst case. The roughness was substantially reduced in Case 3 as compared to Case 1. Thus, the spraying of paint uniformly over the cross section of the panel showed significant improvement in the film topology.

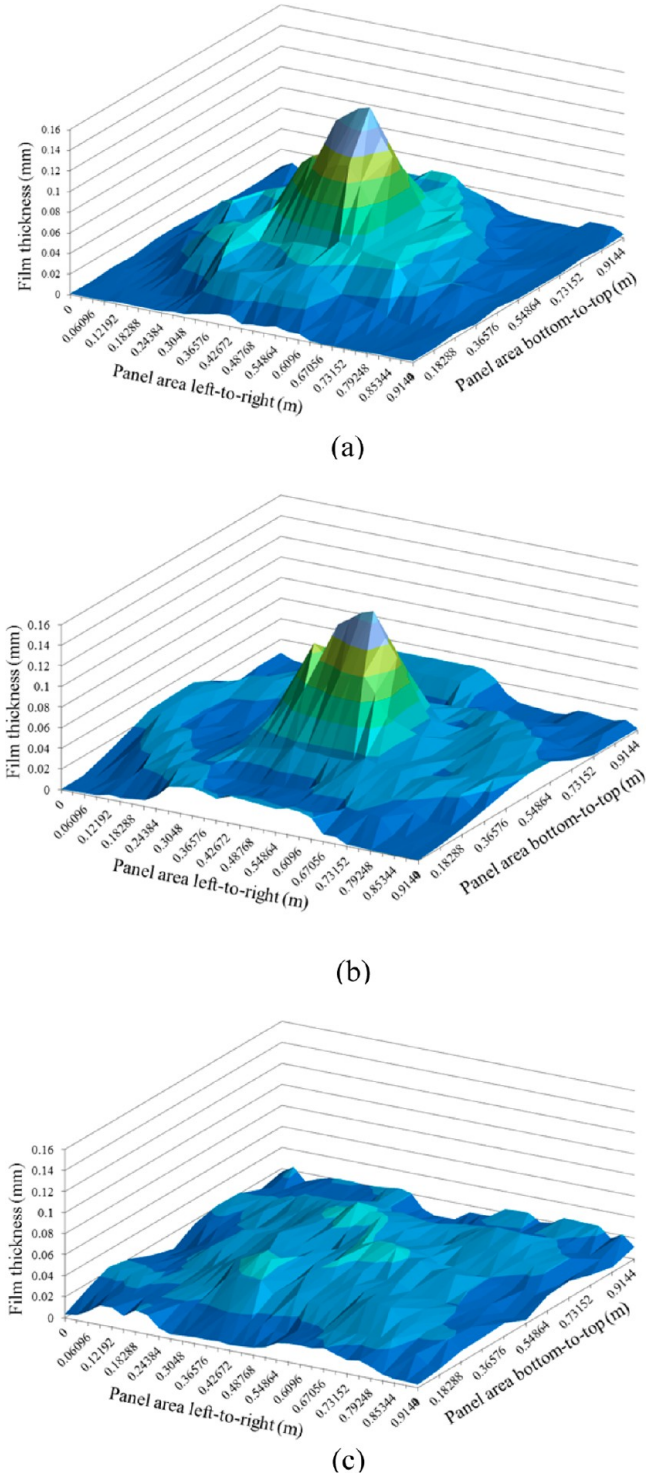


**Figure 10.** Film thickness profiles of nanopaint I from (a) Case 1, (b) Case 2, and (c) Case 3.

## CONCLUDING REMARKS

In the life cycle of a nanocoating, the paint spray stage leads to the highest amount of nanoparticle emission and energy consumption. In this paper, CFD-based modeling and simulation have been performed to analyze the paint spray technique and compare the performance of nanopaint with conventional paint. The case studies are prepared by changing the spray patterns of the deposition of paint material on the receiving panels. The nanopaint spray demonstrated improved transfer efficiency as compared to regular paint under the same operating conditions. However, the ventilation system's performance was worse in the case of nanopaint. The ventilation system required more energy consumption to maintain the quality of the booth air to the same level as that in the case of conventional paint spray. The nanopaint also

shows a better film surface topology as compared to that of conventional paint film.

A comprehensive sustainability assessment of nanocoating technology requires a variety of product and process data. The modeling and simulation technique shown in this work could be very useful for providing such data and to analyze nanocoating systems after the model-based simulation is validated. The modeling and simulation technique is also very useful to predict the performance of the paint spray process in the case of other types of nanomaterials under any specified operating conditions.

## AUTHOR INFORMATION


### Corresponding Author

*Phone: 313-577-3771. Fax: 313-577-3810. E-mail: yhuang@wayne.edu.


### Notes

The authors declare no competing financial interest.

## ACKNOWLEDGMENTS

This work was in part supported by NSF (CBET 1140000 and 1245302).

## REFERENCES


(1) Chow, W. S.; Mohd Ishak, Z. A. Mechanical, morphological and rheological properties of polyamide 6/organo-montorillonite nanocomposites. *Polym. Lett.* **2007**, *1* (2), 77−83.

(2) Nobel, M. L.; Mendes, E.; Picken, S. J. Acrylic-based nanocomposite resins for coating applications. *J. Appl. Polym. Sci.* **2007**, *104*, 2146−2156.

(3) Fang, Z. H.; Duan, H. Y.; Zhang, Z. H.; Wang, J.; Li, D. Q.; Huang, Y. X.; Shang, J. J.; Liu, Z. Y. Novel heat-resistance UV curable waterborne polyurethane coatings modified by melamine. *Appl. Surf. Sci.* **2011**, *257*, 4765−4768.

(4) Dincer, I.; Tozkoparan, O.; German, S. V.; Markin, A. V.; Yildirim, O.; Khomutov, G. B.; Gorin, D. A.; Venig, S. B.; Elerman, Y. Effect of the number of iron oxide nanoparticle layers on the magnetic properties of nanocomposite LbL assemblies. *J. Magn. Magn. Mater.* **2012**, *324*, 2958−2963.

(5) Khanna, A. S. Nanotechnology in high performance paint coatings. *Asian J. Exp. Sci.* **2008**, *21*, 25−32.

(6) Judeinstein, P.; Sanchez, C. Hybrid organic-inorganic materials: A land of multidisciplinary. *J. Mat. Chem.* **1996**, *6*, 511−525.

(7) Lewisky, N. Nanomaterials: What are the environmental and health impacts. *Chem. Eng. Prog.* **2008**, 37−40.

(8) Napierska, D.; Thomassen, L. C. J.; Lison, D.; Martens, J. A.; Hoet, P. H. The nanosilica hazard: Another variable entity. *Part. Fibre Toxicol.* **2010**, *7*, 32.

(9) Schrand, A. M.; Rahman, M. F.; Hussain, S. F.; Schlager, J. J.; Smith, D. A.; Syed, A. F. Metal-based nanoparticles and their toxicity assessment. *WIREs Nanomed. Nanobiotechnol.* **2010**, *2*, 544−568.

(10) Colbert, S. A.; Cairncross, R. A. A discrete droplet transport model for predicting spray coating patterns of an electrostatic rotary atomizer. *J. Electrostat.* **2006**, *64*, 234−246.

(11) Feldman, R. G.; Ratner, M. H.; Ptak, T. Chronic toxic encephalopathy in a painter exposed to mixed solvents. *Environ. Health Perspect.* **1999**, *107*, 417−422.

(12) Kim, B. R.; Kalis, E. M.; DeWulf, T.; Andrews, K. M. Henry's law constants for paint solvents and their implications on volatile organic compound emissions from automotive painting. *Water Environ. Res.* **2000**, *72*, 65−742.

(13) Dunnett, S. J. Numerical study of the factors affecting worker exposure to contaminant. *J. Aerosol Sci.* **1994**, *25*, 481−482.

(14) Reijnders, L. The release of $TiO_2$ and $SiO_2$ nanoparticles from nanocomposites. *Polym. Degrad. Stab.* **2009**, *94*, 873−876.

(15) Li, J.; Uttarwar, R. U.; Huang, Y. L. CFD-based modeling and design for energy-efficient VOC emission reduction in surface coating systems. *Clean Technol. Environ. Policy* **2013**, DOI: 10.1007/s10098-013-0583-9.

(16) Flynn, M. R.; Sills, E. D. On the use of computational fluid dynamics in the prediction and control of exposure to airborne contaminants: An illustration using spray painting. *Ann. Occup. Hyg.* **2000**, *44*, 191−202.

(17) Fogliati, M.; Fontana, D.; Garbero, M.; Vanni, M.; Baldi, G. CFD Simulation of paint deposition in an air spray process. *J. Coat. Technol.* **2006**, *3*, 117−125.

(18) Lu, W. A.; Howarth, T. Numerical analysis of indoor aerosol particle deposition and distribution in two-zone ventilation system. *Build. Environ.* **1996**, *31*, 41−50.

(19) Li, J.; Xiao, J.; Huang, Y. L.; Lou, H. H. Integrated process and product analysis: A multiscale approach to paint spray. *AIChE J.* **2007**, *53*, 2841−2857.

(20) Klaine, S. J.; Alvarez, P. J.; Batley, G. E.; Fernandes, T. F.; Handy, R. D.; Lyon, D. Y.; Mahendra, S.; McLaughlin, M. J.; Lead, J. R. Nanomaterials in the environment: Behavior, fate, bioavailability, and effects. *Environ. Toxicol. Chem.* **2008**, *27*, 1825−1851.

(21) Ellwood, K.; Braslaw, J. A finite-element model for an electrostatic bell sprayer. *J. Electrostat.* **1998**, *45*, 1−23.

(22) Shah, U.; Zhang, C.; Zhu, J. Comparison of electrostatic fine powder coating and coarse powder coating by numerical simulations. *J. Electrostat.* **2006**, *64*, 345−354.

(23) Boulet, M.; Marcos, B.; Dostie, M.; Moresoli, C. CFD modeling of heat transfer and flow field in a bakery pilot oven. *J. Food Eng.* **2010**, *97*, 393−402.

(24) *Ansys Fluent Theory Guide*, version 12.0; Ansys, Inc.: Canonsburg, PA, 2009.

(25) Im, K. S.; Lai, M. C.; Yu, S. T. Simulation of spray transfer processes in electrostatic rotary bell sprayer. *J. Fluids Eng.* **2004**, *126*, 449−456.

(26) Perry, R. H.; Green, D. W. *Perry's Chemical Engineers' Handbook*, 7th ed.; McGraw-Hill: New York, 1997.

(27) Product Stewardship Manual: Safe Handling and Storage, May 2007, Dow. www.dow.com/scripts/litorder.asp?filepath=/296-00312.pdf.

(28) Huynh, N. T. X.; Hoang, V. V.; Zung, H. Structural Properties of Amorphous $SiO_2$ Nanoparticles; College of Natural Sciences of HochiMinh City, Polytechnic Institute of HochiMinh City: HochiMinh City, Vietnam, 2006.

(29) Alderliesten, M. Mean particle diameters. Part VII. The Rosin−Rammler size distribution: Physical and mathematical properties and relationships to moment-ratio defined mean particle diameters. *Part. Part. Syst. Charact.* **2013**, *30*, 244−257.